Electronic spectroscopy of $He@C_{60}^{+}$ for astrochemical consideration

E. K. Campbell[1], E. S. Reedy[1], J. Rademacher[1]

[1] School of Chemistry, University of Edinburgh, Joseph Black Building, Kings Buildings, David Brewster Road, Edinburgh EH9 3FJ, UK

e.k.campbell@ed.ac.uk, e.s.reedy@sms.ed.ac.uk, j.rademacher@sms.ed.ac.uk

R. J. Whitby[2], G. Hoffman[2]

[2] Chemistry, University of Southampton, Southampton, HANTS, SO17 1BJ, UK

r.j.whitby@soton.ac.uk, g.hoffman@soton.ac.uk

Received _____; accepted _____

ABSTRACT

The electronic spectrum of the endohedral fullerene $He@C_{60}^+$ observed by messenger spectroscopy in a cryogenic ion trap is presented. The role played by the messanger tag in the adopted experimental method is evaluated by recording spectra of $He@C_{60}^+ - He_n$ with $n = 1 - 4$. The results indicate a linear shift of ~ 0.7 Å in the wavelengths allowing accurate gas phase values to be **reported**. The presence of the helium inside the cage shifts the absorption bands by $2 - 3$ Å toward shorter wavelengths compared to C_{60}^+. The magnitude of this displacement will enable searches for the spectral signatures of this fullerene analogue in interstellar environments by absorption spectroscopy. The implications for potential astronomical detection are discussed.

Subject headings: ISM: general - ISM: lines and bands - ISM: molecules

1. Introduction

Around the time of the discovery of the fullerenes and the stability of their cage structures, the possible relevance of C_{60} to the diffuse interstellar band (DIB) enigma was recognized (Kroto et al. 1985). Given the low ionization potential of C_{60} and the harsh radiation field in the interstellar medium (ISM), in 1987 the cation C_{60}^+ was predicted to be an important interstellar molecule (Kroto 1987). A convincing association of C_{60}^+ absorptions with several near-infrared DIBs was accomplished much later through the comparison between observational data and laboratory spectra recorded under conditions relevant to the ISM.

Electronic spectra of C_{60}^+ embedded in low temperature matrices were reported by several groups, with the best resolved study in neon (D'Hendecourt et al. 1992; Fulara et al. 1993) providing data that enabled a prediction of the wavelengths at which gas phase C_{60}^+ would absorb. This facilitated a search by Foing & Ehrenfreund (1994) in the spectra of reddened stars for two prominant bands, and led them to propose that two DIBs at 9577 and 9632 Å are caused by this molecular ion. 21 years later Maier and colleagues (Campbell et al. 2015) produced gas phase spectroscopic data on C_{60}^+ suitable for a direct comparison with astronomical data. These results**, obtained by fragmentation of** $C_{60}^+ - He$ **in a cryogenic trap,** showed a striking match to the two reported DIBs (Foing & Ehrenfreund 1994).

Subsequently, evidence for weaker absorption features identified in the laboratory electronic spectrum of $C_{60}^+ -$ **He** were searched for. This led to the detection and attribution of two additional DIBs at 9428 and 9365 Å to C_{60}^+ (Walker et al. 2015). Further development of the cryogenic ion trapping instrument provided the opportunity to refine the laboratory absorption characteristics and enable the measurement **of** absolute absorption cross-sections (Campbell et al. 2016a,b). This allowed direct determination of

the column density of C_{60}^+ toward HD 183143, $N(C_{60}^+) = 2 \times 10^{13}\,\mathrm{cm}^{-2}$. Observational data showing a weak interstellar DIB at 9345 Å coinciding with a C_{60}^+ absorption was also presented. Concurrently, refinements in the analysis of the astronomical observations were shown to yield closer agreement between laboratory and astronomical data (Walker et al. 2016). Although some objections to the identification of C_{60}^+ as a DIB carrier were raised (Galazutdinov et al. 2017), the conclusions reached in this observational study were refuted by Walker et al. (2017) and also by another, independent, group (Lallement et al. 2018).

Recently, observational data obtained with the *Hubble Space Telescope* were reported (Cordiner et al. 2017, 2019). Although relatively low resolution, these measurements were able to eliminate the considerable uncertainity in the analysis of observational data in this spectral region caused by telluric H_2O lines. In the latter study, Cordiner et al. (2019) were able to clearly show the presence of intrinsically weak C_{60}^+ absorptions in the interstellar spectrum, supporting the identifications orignally made by Walker et al. (2015). Moreover, on the laboratory side, the conclusions reached regarding the wavelengths of C_{60}^+ absorptions from the cryogenic ion trapping measurements were corroborated by independent experiments using a different technique (Kuhn et al. 2016; Spieler et al. 2017). The situation was reviewed recently by Maier & Campbell (2018).

Identification of C_{60}^+ as a DIB carrier naturally led to questions concerning the role played by other fullerenes and analogues with respect to other unidentified interstellar absorptions. A nice discussion of relevant molecular species has been given by Omont (2016). The second most abundant fullerene produced in the usual electric arc discharge of carbon rods or laser vaporisation synthesis is C_{70}^+. Similar to C_{60}^+ this ion satisfies the isolated pentagon rule used to explain the stability of these molecules. C_{70} also has a low ionization potential, suggesting that if present in diffuse clouds, one might also

anticipate that, in certain regions, it would be in ionized form. The gas phase spectrum of $C_{70}^+ - \mathbf{He}$ reported by Campbell et al. (2016a) in the region $7000 - 8000\,\text{Å}$ showed that the intensity of the electronic transition is spread out over many features of roughly equal strength. Unlike the pattern for C_{60}^+, in which the electronic band oscillator strength is localised in two features, the appearance of the C_{70}^+ spectrum precludes interstellar detection because each absorption band has a relatively small absorption cross-section ($\sim 10^{-17}\,\text{cm}^2$). Another example is C_{70}^{2+}. Although in this case most of the intenstity of the $^3E_1' \leftarrow X\,^3A_1'$ electronic transition near 7000 Å is contained in the origin band, the broad width ($\sim 35\,\text{Å}$) of the absorption makes astronomical searches difficult, especially with echelle spectrographs (Campbell et al. 2017). This result means that to date it has not been possible to evaluate the size distribution of interstellar fullerenes in the diffuse ISM.

Although all fullerenes except C_{60}^+ for which accurate gas phase data is available have been shown to possess unfavourable characteristics for astronomical detection, the sample set is small. Based on the high abundance of C_{60}^+ in interstellar environments, $N(C_{60}^+) = 2 \times 10^{13}\,\text{cm}^{-2}$ toward HD 183143, one might expect the presence of other fullerenes and/or analogues. For example, it has been shown through experiments that many analogues form as readily as the bare carbon **structures** under the usual laboratory synthesis conditions. These include endohedral, exohedral as well as heterofullerenes. We recently built an apparatus in order to synthesize and characterize analogues that have not yet been produced and isolated in macroscopic quantities and demonstrated its use by obtaining low temperature spectroscopic data on gas phase C_6^+ (Campbell & Dunk 2019).

Evidence that He could be incorporated inside the fullerene cation C_{60}^+ to yield the endohedral analogue, denoted $He@C_{60}^+$, was presented following high energy collisions of C_{60}^+ and He in a tandem mass-spectrometer (Weiske et al. 1991). Macroscopic quantities of the neutral $He@C_{60}$ were originally prepared with very low incorporations of He in the

sample ($< 0.1\,\%$) by heating C_{60} under a high pressure of the inert gas (Saunders et al. 1994). Subsequently, advances in synthetic chemical methods led to the production of a few endohedral fullerenes that possess rare gas atoms or small molecules inside the cage with high incorporation using what is known as the molecular surgery approach, including H_2 (see Murata et al. (2008) and Krachmalnicoff et al. (2014)), HF (Krachmalnicoff et al. 2016), and He (Morinaka et al. 2010).

Recently, the electronic spectrum of $H_2@C_{60}^+$ in the gas phase was presented (Strelnikov et al. 2018). This was obtained by photofragmentation of $\mathbf{H_2@C_{60}^+ - He}$ in a wire quadrupole trap. The data showed a clear distinction from the absorptions of C_{60}^+ in terms of the wavelengths of the band maxima, however, the spectrum was recorded with a step size of 2.5 Å, which is comparable to the natural widths of the near infrared electronic C_{60}^+ transitions. The high laser fluence used in these experiments led to a strong saturation broadening of the absorptions. A preliminary search in catalogues did not reveal identification of any DIBs at the predicted $H_2@C_{60}^+$ wavelengths and an upper limit of $10\,\%$ of the C_{60}^+ abundance was suggested.

In this contribution spectroscopic data on the endohedral fullerene $He@C_{60}^+$ is reported. This system was chosen **because helium is the second most abundant element in the universe and the high pressures and temperatures needed to form C_{60} are likely to encourage helium inclusion.** Section 2 describes the experimental procedure**, results are presented in Section 3, implications for astronomical detection are given in Section 4 and conclusions in Section 5.**

2. Experimental

30 % filled ^{4}He@C_{60} was synthesised using a variation (Hoffman et al. 2020) in the method reported for H_2@C_{60} by Krachmalnicoff et al. (2014). Spectroscopic experiments were carried out with the cryogenic ion trap apparatus described **in Campbell et al. (2016a) and Campbell & Dunk (2019)**. A few mg of 30 % filled ^{4}He@C_{60} was heated in an oven to 350 °C. Singly charged cations were generated by 40 eV electron impact ionisation of the neutral gas. Figure 1 shows the mass spectrum obtained by operating the first quadrupole mass spectrometer in transmission mode and scanning the second. These results indicate that most of the ions with $m/z = 724$ are due to ^{4}He@$^{12}C_{60}^+$, with only a small contribution from $^{13}C_4^{12}C_{56}^+$, and that this 'contamination' can safely be neglected in the following analysis.

Ions with $m/z = 720 - 723$ were removed from the beam injected into the trap using the first quadrupole mass-spectrometer. This allowed the spectrum shown in Figure 1 to be recorded. This was obtained at a nominal trap temperature, $T_{\rm nom} = 3.9$ K and with a helium number density of 10^{15} cm^{-3}. Under these conditions a significant number of primary He@C_{60}^+ ions are converted into He@$C_{60}^+ - {\rm He_n}$ complexes. To generate Figure 1, He@C_{60}^+ were loaded into the trap for 200 ms by lowering the potential applied to the axial entrance electrode. During the first 500 ms they interact with helium buffer gas, which was subsequently pumped out for 420 ms before the trap contents were extracted and analysed by the second quadrupole mass-spectrometer. The trapping process was repeated at a repetition rate of 1 Hz.

To obtain photofragmentation spectra of He@$C_{60}^+ - {\rm He_n}$ complexes the ion cloud was exposed to radiation provided by a continuous wave (cw) Ti:Sap laser. The exposure time of 30 ms, occuring a few ms before extraction, was controlled using a mechanical shutter. The number of ions were monitored on alternate storage cycles with ($N_{\rm i}$) and without (N_0) exposure to laser radiation in order to account for long term stability of the number of ions

loaded into trap. The cw laser power was monitored using a power meter to account for changes to the photon fluence as a function of wavelength. The analysis of experimental data follows that described in Campbell et al. (2016a).

3. Results

The origin bands in the electronic spectrum of $He@C_{60}^+ - He$ are shown in Figure 2. The profiles were recorded at a laser fluence that resulted in attenuation $(1 - N_i/N_0) < 25\,\%$, in order to provide information on their natural width. Also shown are fits to the data with Lorentzians; a single function with wavelength 9574.9 Å and FWHM 1.9 Å was used on the shorter wavelength absorption. For the lowest energy band, two functions are necessesary to fit the contour, these have wavelengths, 9630.5 and 9632.2Å, and widths, 1.3 and 1.2 Å, respectively. Apart from a wavelength shift of $2 - 3$ Å this analysis gives very similar results to the evaluation of $C_{60}^+ - He$ data described by Campbell & Maier (2018).

In order to rule out calibration or other systematic errors as the source of the shift, the spectrum of $^{12}C_{60}^+ - He$ was recorded under identical laboratory conditions. This could be easily achieved due to the abundance of $^{12}C_{60}^+$ in the sample (see Figure 1). Mass-selection of $m/z = 720$ using the first quadrupole allowed $^{12}C_{60}^+ - He$ complexes to appear at $m/z = 724$ without contamination from $^4He@^{12}C_{60}^+$. The resulting fragmentation spectrum of $^{12}C_{60}^+ - He$ in the region of the two origin bands is shown in Figure 2 along with that of $He@C_{60}^+ - He$, clearly indicating differences in the wavelength of band maxima upon encapsulation of a helium atom within the cage. As the two sets of data also show the same attenuation at band maxima under conditions of identical laser fluence, the corresponding absorption cross-sections are very similar.

To provide information on the perturbation caused to the $He@C_{60}^+$ electronic spectrum

due to the presence of the weakly bound exohedral helium atom, photofragmentation spectra of $He@C_{60}^+ - He_n$, with $n = 1 - 4$ have been recorded in the region of the band near 9575 Å. Data recorded on the $m/z = 728, 732, 736$, and 740 mass channels are shown in Figure 3. The $n = 1 - 4$ absorption bands have each been fit with a single Lorentzian function, yielding wavelengths at band maxima of 9575.1, 9575.8, 9576.5, 9577.2 Å, and widths 2.2, 2.6, 3.0, and 3.5 Å, respectively. The former values are plotted as a function of n in Figure 3. As indicated, these show a linear behaviour, allowing extrapolation to $n = 0$. The predicted value for $He@C_{60}^+$ based on this analysis is 9574.4 Å. The slope of the linear fit indicates a shift per helium atom of 0.7 Å, in agreement with the results found previously for C_{60}^+ in both ion trapping (Campbell et al. 2016b) and helium droplet experiments (Kuhn et al. 2016). The increasing FWHM of the bands with n is believed to be due to isomeric broadening, as described in Kaiser et al. (2018).

The electronic spectrum of $He@C_{60}^+ - He$ encompassing the region containing the first 5 absorption bands is presented in Figure 4. Also shown are the corresponding $C_{60}^+ - He$ absorptions reported by Campbell & Maier (2018). The spectra of these two ions are nearly superimposable, aside the wavelength shift. **The predicted band maxima of the** $He@C_{60}^+$ **absorptions are listed in Table 1. The values are obtained by applying a** 0.7 Å **shift (caused by the weakly bound helium atom) to the fits shown in Figure 4. Note that small uncertainties in these wavelengths, in the order of** $0.1 - 0.2$ Å**, arise due to the experimental conditions (e.g. laser fluence) and deviations of the band profiles from single Lorentzian functions. The extrapolated** $He@C_{60}^+$ **values are** compared with those predicted for C_{60}^+ in Table 1. Inspection of the two data sets reveals a blue shift of $2 - 3$ Å due to the endohedral helium atom. This is $3 - 4$ times larger than the 0.7 Å magnitude perturbation caused by the exohedrally bound atom.

4. Astronomical Implications

The $2-3$ Å wavelength shift relative to absorption bands of C_{60}^+ leads to the question as to whether one might be able to search for distinct DIBs due to He@C_{60}^+. To investigate this, simulated spectra of a mixture of C_{60}^+ and He@C_{60}^+ are shown in Figure 5. These plots indicate the appearance of the profiles resulting from C_{60}^+, and He@C_{60}^+ + C_{60}^+, with the endohedral molecular ion present at abundance of 0.1 and 0.2 relative to that of the empty cage. The data used in Figure 5 are from fits to helium tagged spectra of He@C_{60}^+ and C_{60}^+, shifted to take into account the wavelength perturbation caused by the exohedrally bound helium atom, as determined in this paper and Campbell et al. (2016a). The contributions from He@C_{60}^+ in the combined spectra results in weak satellites appearing on the short wavelength wings of the C_{60}^+ absorptions.

As shown in Figure 5, due to the widths of the C_{60}^+ and He@C_{60}^+ absorptions, their spectra are overlapped. The FWHM of the laboratory absorptions recorded at temperatures below 10 K has been interpreted as due to the picosecond lifetime of the exctied electronic state, however, it should be noted that further broadening due to the rotational envelope will occur at tempertures in the range $50-80$ K expected for non-polar molecules in the diffuse ISM (Campbell & Maier 2018). For example, an increase in the FWHM from $\sim$ 2 Å (below 10 K) to $\sim$ 4 Å at 100 K **in the near infrared** is expected (Edwards & Leach 1993; Ehrenfreund & Foing 1996). **Foing & Ehrenfreund (1997) measured the FWHM of the C_{60}^+ DIBs at 9632 and** 9577 Å **to be** 2.8 Å **in diffuse clouds toward** HD 183143**, and** 4 Å **in ESO spectra along the line-of-sight toward** HD 37022**, consistent with a temperature of** 130 ± 30 K**.** An increase in the FWHM due to the rotational envelope in interstellar spectra may make distinguishing C_{60}^+ absorptions from He@C_{60}^+ contributions more challenging.

The spectral region containing the C_{60}^+ bands is strongly polluted by telluric water

lines in the available ground-based high-resolution observational data. This makes searches for weaker 'satellites' near the C_{60}^+ absorptions difficult. Along the line-of-sight towards HD 183143, where the 9577 DIB due to C_{60}^+ causes a strong $\sim$ 10 % attenuation in starlight, a weak band near 9362 Å is observed. This lies very close to the wavelength of the He@C_{60}^+ absorption. However, the evaluated CFHT ESPaDOnS data (Walker et al. 2015, 2016) around the 9577 DIB does not show a clear absorption at 9574 Å, where the strongest He@C_{60}^+ band should appear. Moreover, in the best available data on the 9632 DIB (CFHT f/8 reported in Foing & Ehrenfreund (1997)), there is no clear indication of a He@C_{60}^+ band near 9630 Å. Inspection of the recent lower resolution observational data collected with the *Hubble Space Telescope* gives a similar result for the regions around the DIBs at 9577 and 9365 Å.

The lack of a clear cut identification of interstellar absorptions due to He@C_{60}^+ should enable upper limits to be placed on its column density. However, careful corrections are needed to evaluate observational data, due to background telluric water lines, stellar features and/or other interstellar absorptions. Given these severe observational constraints, estimates of abundance limits are not given here. Rather, in Table 1 the wavelengths of the laboratory He@C_{60}^+ absorptions are listed to facilitate future searches when appropriate background free high signal-to-noise data containing the strongest absorption bands **become** available.

5. Conclusions

Near-infrared absorptions of the endohedral fullerene cation He@C_{60}^+ in the vicinity of the electronic transitions of the C_{60}^+ cage were measured below 10 K in a cryogenic trap. The encaspulated helium atom causes the spectrum to shift by $2 - 3$ Å relative to that of C_{60}^+. Apart from this difference in the wavelengths, the other spectral characteristics, including

absolute absorption cross-sections at band maxima, are found to be very similar to those of C_{60}^+. The potential for astrochemical detection is discussed and it is concluded that at present the available observational data is not sufficient for a conclusive search for the presence of $He@C_{60}^+$ in diffuse clouds. Further high resolution background free observations are recommended to facilitate astronomical detection or enable accurate upper limits to be placed on the column density of this fullerene analogue.

The authors thank G. A. H. Walker for discussions and acknowledge financial assistance from the Royal Society (URF/R1/180162, RGF/EA/181035) and EPSRC (EP/P009980/1).

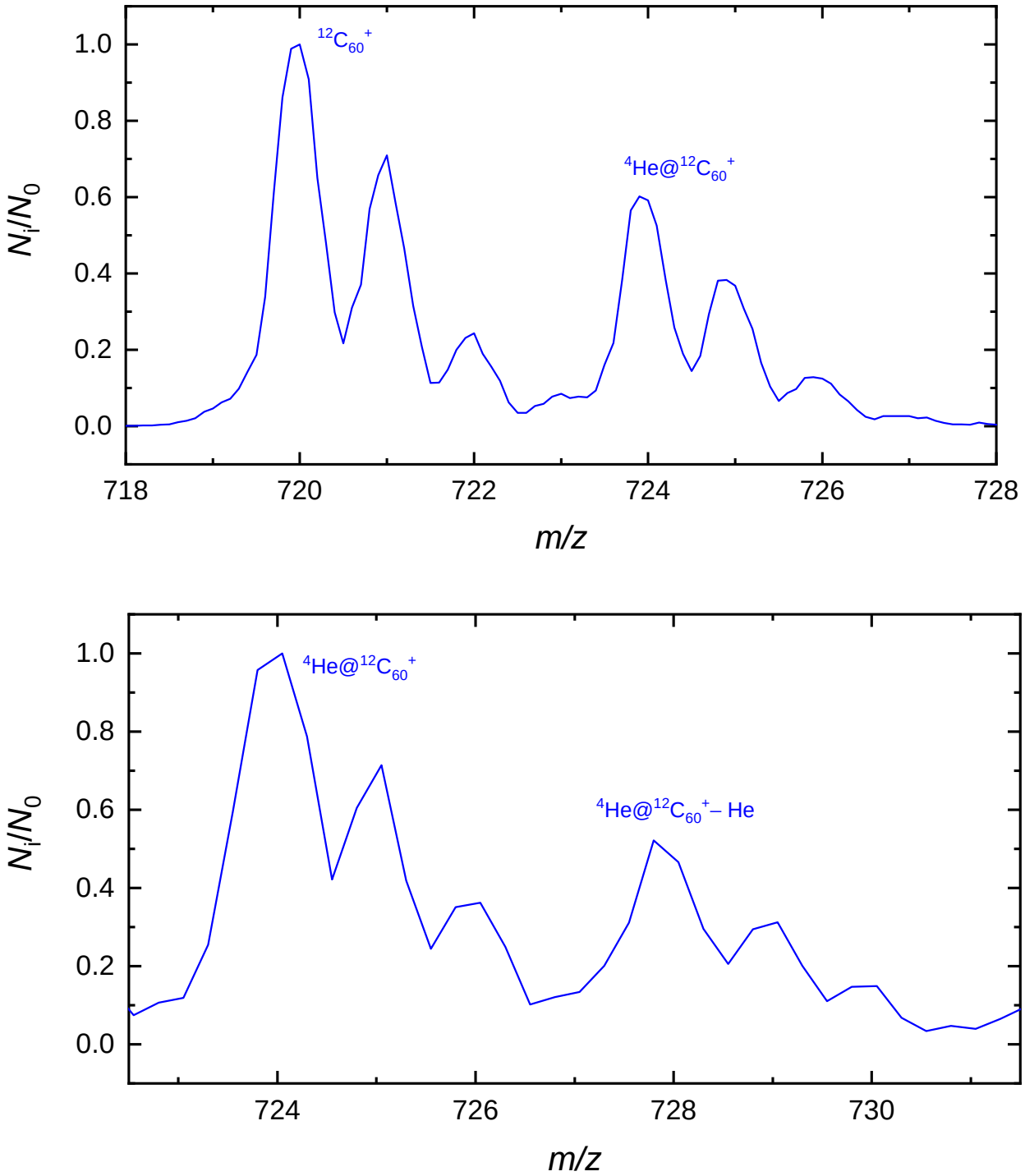

Fig. 1.— (Top) Mass-spectrum of $He@C_{60}^{+}$ sample used in this work. This indicates that under the conditions used most of the ions appearing at m/z = 724 are $^{4}He@C_{60}^{+}$.

(Bottom) Mass-spectrum of $He@C_{60}^{+}$ ions stored in cold (3.9 K) and dense (10^{15} cm^{-3}) buffer gas. The data indicate the formation of $He@C_{60}^{+}$ – He.

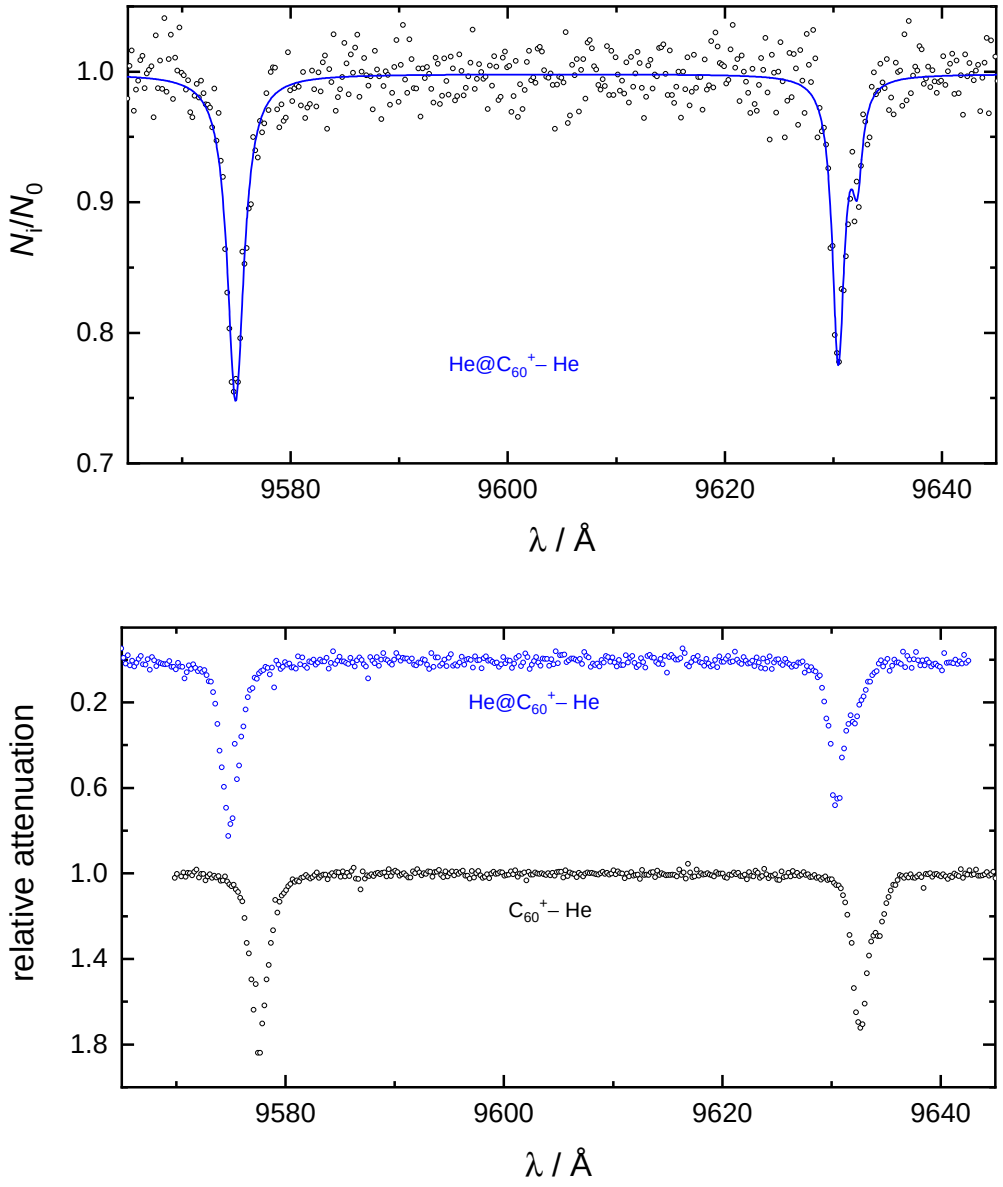

Fig. 2.— (Top) Absorptions of $\mathrm{He@C_{60}^+} - \mathrm{He}$ measured with attenuation $(1 - N_\mathrm{i}/N_0) < 25\,\%$. The circles are the experimental data while the solid blue line is the cumulative result obtained from fitting the data with three Lorentzians. The wavelengths and widths of these functions are 9574.9 Å and 1.9 Å, 9630.5 Å and 1.3 Å, and 9632.2 Å and 1.2 Å, respectively.

(Bottom) Absorptions of $\mathrm{He@C_{60}^+} - \mathrm{He}$ (blue) and $\mathrm{C_{60}^+} - \mathrm{He}$ (black) measured under the same laboratory conditions. The y-axes of the $\mathrm{C_{60}^+} - \mathrm{He}$ data has been offset for clarity. See the text for a discussion.

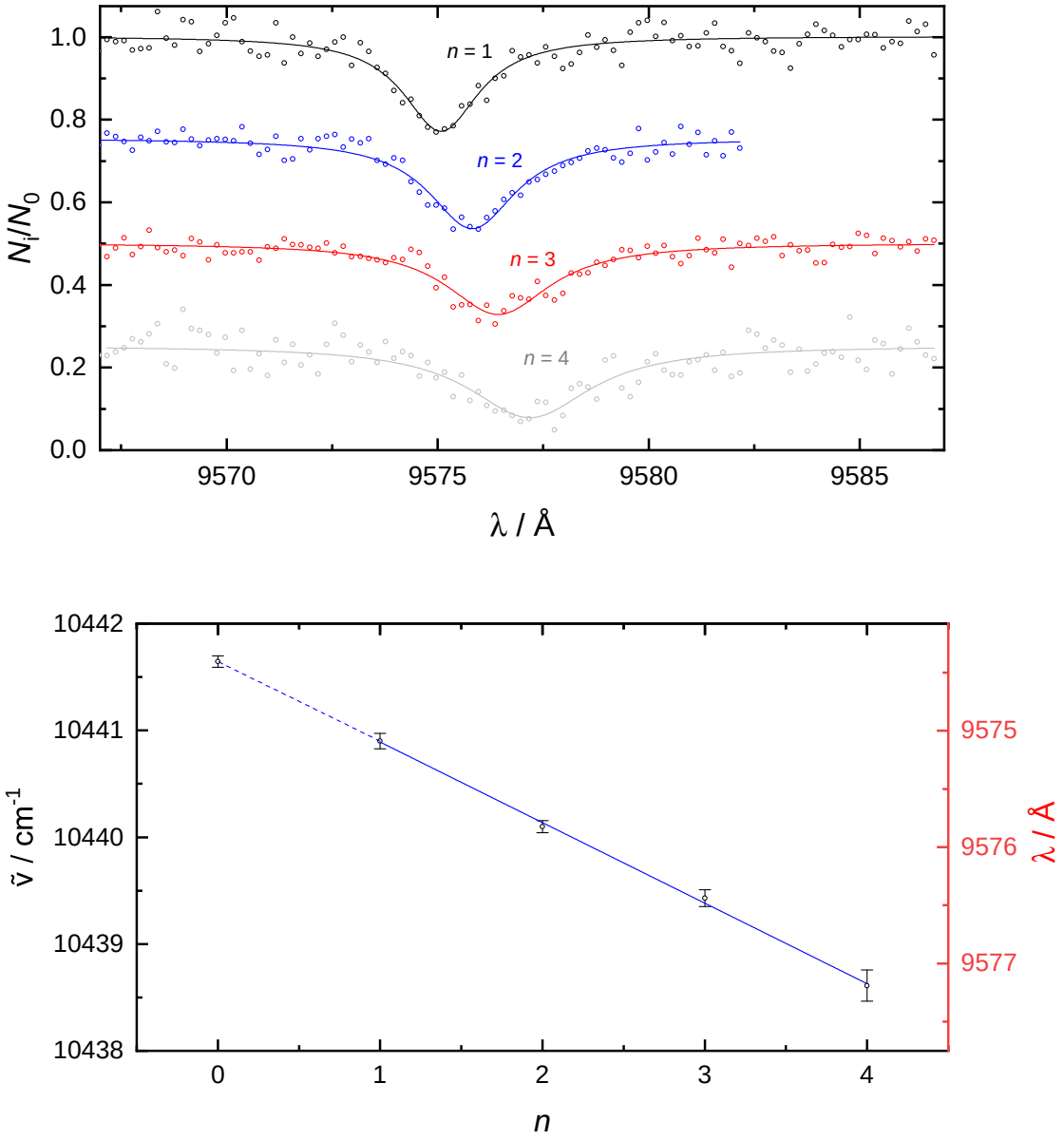

Fig. 3.— (Top) Absorptions of $He@C_{60}^+ - He_n$ $(n = 1 - 4)$. The circles are experimental data and solid lines are Lorentzian functions. These fits indicate band maxima at 9575.1, 9575.8, 9576.5, 9577.2 Å and widths of 2.2, 2.6, 3.0, and 3.5 Å, for $n = 1, 2, 3$ and 4, respectively. The y-axes of the $n = 2 - 4$ data have been offset for clarity.

(Bottom) Linear fit (solid line) to the $He@C_{60}^+ - He_n$ $(n = 1 - 4)$ laboratory absorptions (circles). The data are from the Lorentzian fits to the spectra shown in Figure 3. The intercept implies that the absorption of $He@C_{60}^+$ has band maximum at 9574.4 Å. The slope indicates that the redshift per helium atom is 0.7 Å.

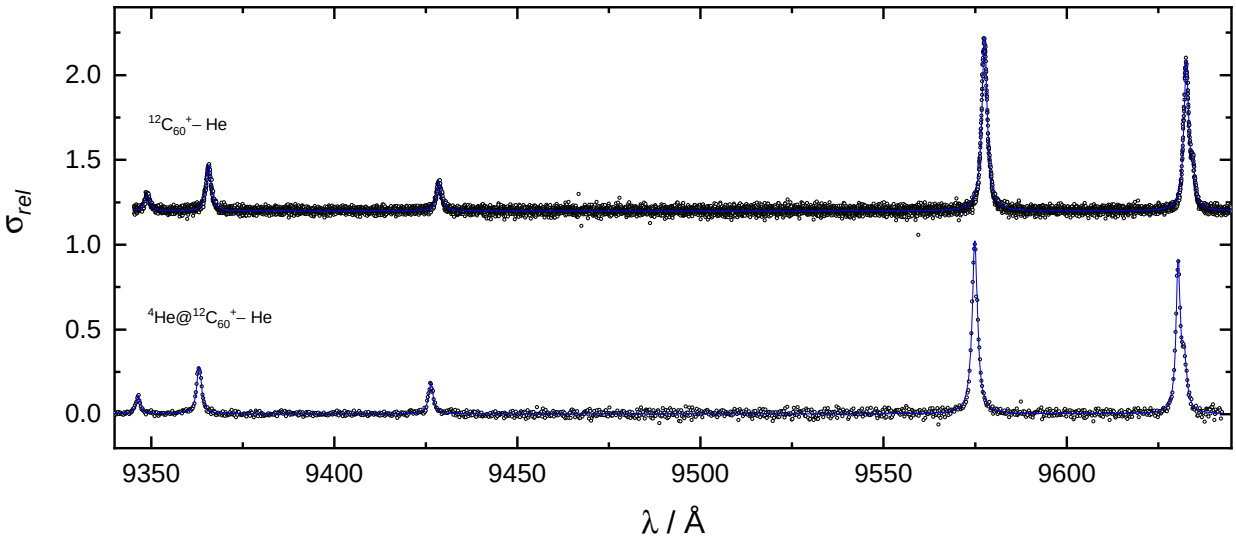

Fig. 4.— He@C_{60}^+−He photofragmentation spectrum recorded by monitoring the attenuation of ions with $m/z = 728$ (bottom). It is compared with data on $C_{60}^+ - He$ reported previously (Campbell & Maier 2018) (top). The experimental data (circles) have been fit with Lorentzian profiles, the cumulative result is the solid blue line.

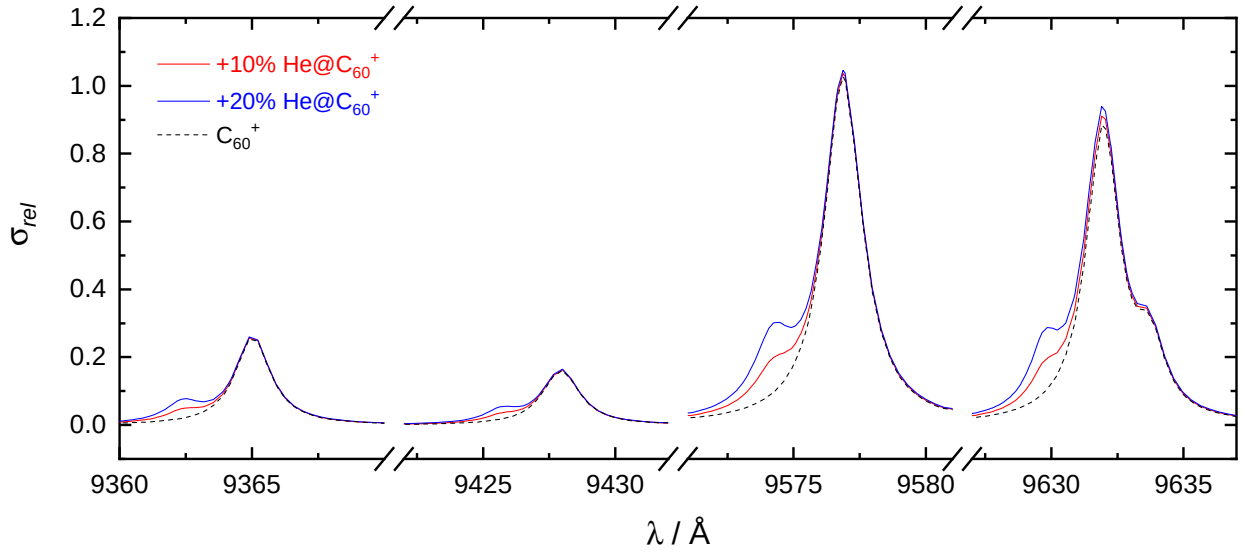

Fig. 5.— Absorption band profiles of C_{60}^+ (black), and $He@C_{60}^+$: C_{60}^+ mixtures in ratios 0.1:1 (red) and 0.2:1 (blue). The data are from the fits shown in Figure 4 with wavelengths shifted to take into account the perturbation caused by the weakly bound Helium atom.

Table 1. **Absorption wavelengths inferred from laboratory measurements**

λ_c ($He@C_{60}^+$)† / Å	λ_c (C_{60}^+)†† / Å	Δ / Å	σ_{rel} †††
9629.7 ±0.2	9632.1 ±0.2	2.4	0.84
9574.**4** ±0.2	9577.0 ±0.2	2.**6**	1.00
9425.7 ±0.2	9427.8 ±0.2	2.1	0.17
9362.4 ±0.2	9365.2 ±0.2	2.8	0.26
9345.7 ±0.2	9348.4 ±0.2	2.7	0.09

† **Wavelength and uncertainty of** 9574.4 ± 0.2 Å **is from linear fit shown in Figure 3. The other wavelengths are extrapolated from** $He@C_{60}^+ - He$ **data shown in Figure 4.**

† † Extrapolated C_{60}^+ wavelengths taken from Campbell et al. (2016b).

† † † Values are the band maxima in the measured $C_{60}^+ - He$ spectrum taken from Campbell & Maier (2018).

REFERENCES

Campbell, E. K., Holz, M., Gerlich, D., & Maier, J. P. 2015 Nature, 523, 322.

Campbell, E. K., Holz, M., Maier, J. P., Gerlich, D., Walker, G. A. H. & Bohlender, D. 2016 ApJ, 822, 17.

Campbell, E. K., Holz, M., Maier, J. P. 2016 ApJL, 826, L4.

Campbell, E. K., Holz, M., Maier, J. P. 2017 ApJ, 835, 221.

Campbell, E. K. & Maier, J. P. 2018 ApJ, 858, 36.

Campbell, E. K. & Dunk, P. W. 2019 RSciI, 90, 103101.

Cordiner, M. A., Cox, N. J. L., Lallement, R., Najarro, F., Cami, J., Gulle, T. R., Foing, B. H., Linnartz, H., Lindler, D. J., Proffitt, C. R., Sarre, P. J. & Charnley, S. B., 2017, ApJL, 843, L2.

Cordiner, M. A., Linnartz, H., Cox, N. J. L., Cami, J., Najarro, F., Proffitt, C. R., Lallement, R., Ehrenfreund, P., Foing, B. H., Gull, T. R., Sarre, P. J. & Charnley, S. B., 2019, ApJL, 875, L28.

D'Hendecourt, L., Fostiropoulos, K., Léger, A. published in Joblin PhD, Paris University (1992).

Edwards, S. A., & Leach, S. 1993 A&A, 272, 533.

Ehrenfreund, P. & Foing, B. H. 1996, A&A, 307, L25.

Foing, B. H., & Ehrenfreund, P. 1994, Nature, 369, 296.

Foing, B. H. and Ehrenfreund, P. 1997, A&A, 317, L59.

Galazutdinov, G. A., Shimansky, V. V., Bondar, A., Valyavin, G., & Krelowski, J. 2017 MNRAS, 465, 3956.

Hoffman, G., Grasvik, J., Alom, S., Bacanu, G., Bloodworth, S., Levitt, M. H. & Whitby, R. J. 2020 in preparation.

Fulara, J., Jakobi, M., & Maier, J. P. 1993 CPL, 206, 203.

Kaiser, A., Postler, J., Ončák, M., Kuhn, M., Renzler, M., Spieler, S., Simpson, M., Gatchell, M., Beyer, M. K., Wester, R., Gianturco, F. A., & Scheier, P. 2018 JPCL, 9, 1237.

Krachmalnicoff, A., Levitt, M. H. & Whitby, R. J. 2014 Chem. Commun. 50, 13037.

Krachmalnicoff, A., Bounds, R., Mamone, S., Alom, S., Concistrè, M., Meier, B., Kouřil, K., Light, M. E., Johnson, M. R., Rols, S., Horsewill, A. J., Shugai, A., Nagel, U., Rõõm, T., Carravetta, M., Levitt, M. H., & Whitby, R. J. 2016 NatChem, 8, 953.

Kroto, H. W., Heath, J. R., O'Brien, S. C., Curl, R. F., & Smalley, R. E.1985 Nature, 318, 162.

Kroto, H. W. 1987, in Polycyclic Aromatic Hydrocarbons and Astrophysics, ed. A. Léger & d'Hendecourt (Dordrecht: Riedel), 197.

Kuhn, M., Renzler, M., Postler, J., Rasler, S., Spieler, S., Simpson, M., Linnartz, H., Tielens, A. G. G. M., Cami, J., Mauracher, A., Wang, Y., Alcamí, M., Martín, F., Beyer, M. K., Wester, R., Lindinger, A. & Scheier, P. 2016, Nat. Comm., 7, 13550.

Lallement, R., Cox, N. L. J., Cami, J., Smoker, J., Fahrang, A., Elyajouri, M., Cordiner, M. A., Linnartz, H., Smith, K. T., Ehrenfreund, P. & Foing, B. 2018 A&A, 614, A28.

Maier, J. P. & Campbell, E. K. 2018 IJMS, 434, 2018.

Morinaka, Y., Tanabe, F., Murata, M., Murata, Y. & Komatsu, K. 2010 Chem. Commun. 46, 4532.

Murata, M., Murata, Y. & Komatsu, K. 2008 Chem. Comm., 6083.

Omont, A. 2016 A&A, 590, A52.

Saunders, M., Jiménez-Vázquez, H. A., Cross, R. J., Mroczkowski, S., Gross, M. L., Giblin, D. E. & Poreda, R. J. 1994 JACS, 116, 2193.

Spieler, S., Kuhn, M., Postler, J., Simpson, M., Wester, R., Scheier, P., Ubachs, W., Bacalla, X., Bouwman, J. & Linnartz, H. 2017 ApJ, 846, 168.

Strelnikov, D. V., Jasik, J., Gerlich, D. Murata, M., Murata, Y., Komatsu, K., & Roithova, J. 2018 JPCA, 122, 41.

Walker, G. A. H., Bohlender, D. A., Maier, J. P. & Campbell, E. K. 2015 ApJL, 812, L8.

Walker, G. A. H., Campbell, E. K., Maier, J. P., Bohlender, D. & Malo, L. 2016 ApJ, 831, 130.

Walker, G. A. H., Campbell, E. K., Maier, J. P., & Bohlender, D. 2017 ApJ, 843, 56.

Weiske, T., Böhme, D. K., Hrušák, J., Krätschmer, W., & Schwarz, H. 1991, Angew. Chemie. Int. Ed., 30, 884.